# Self-Assembled Monolayers of Dodecyl and Hydroxy-Dodecyl Phosphates on Both Smooth and Rough Titanium and Titanium Oxide Surfaces

**ARTICLE** *in* LANGMUIR · APRIL 2002

Impact Factor: 4.46 · DOI: 10.1021/La011459p



**4 AUTHORS**, INCLUDING:

Samuele G. P. Tosatti
ETH Zurich
**60** PUBLICATIONS **2,359** CITATIONS
SEE PROFILE

Marcus Textor
ETH Zurich
**333** PUBLICATIONS **13,999** CITATIONS
SEE PROFILE

Nicholas D Spencer
ETH Zurich
**403** PUBLICATIONS **11,606** CITATIONS
SEE PROFILE

# Self-Assembled Monolayers of Dodecyl and Hydroxy-dodecyl Phosphates on Both Smooth and Rough Titanium and Titanium Oxide Surfaces

S. Tosatti, R. Michel, M. Textor,* and N. D. Spencer

*Laboratory for Surface Science and Technology, Department of Materials, Swiss Federal Institute of Technology (ETHZ), CH-8092 Zürich, Switzerland*

*Received September 21, 2001. In Final Form: February 1, 2002*

Dodecyl phosphate and hydroxy-terminated dodecyl phosphate are shown to spontaneously assemble on smooth titanium oxide and titanium metal coated glass and silicon substrates, as well as on rough titanium metal implant surfaces. The surfaces were dipped in aqueous solutions of the corresponding ammonium salts for 48 h. The molecules are shown by X-ray photoelectron spectroscopy (XPS) to form densely packed, self-assembled monolayers (SAMs) on all surfaces investigated. The phosphate headgroups are believed to attach to the titanium (oxide) surface with the terminal end group (either methyl or hydroxy) pointing toward the ambient environment (air, vacuum, or water). Mixed SAMs are shown to be formed from mixed aqueous solutions of the two amphiphiles, with the hydroxy-terminated dodecyl phosphate adsorbing more favorably than the methyl-terminated molecule. The advancing water contact angles can be easily tailored via the composition of the self-assembly solution in the range of 110° (pure methyl) to 55° (pure hydroxy) on flat, smooth titanium surfaces. Surface roughness strongly modifies the wetting properties, with advancing contact angles in the range of 150−100° being observed, as well as the degree of hysteresis (difference between advancing and receding angles). Model calculations based on XPS intensities have been successfully used to quantify the adlayer composition and molecular surface densities across the whole range of mixed adlayer chemistry. The organophosphate monolayers on titanium are believed to have a significant potential for precise control of the surface chemistry and interfacial tension on both smooth and rough titanium surfaces in application areas such as medical implants and other devices where independent control of surface chemistry and topography is essential to performance.

## 1. Introduction

Self-assembled monolayers (SAMs) have attracted a lot of attention, thanks to their ability to form chemically well-controlled, structurally ordered surfaces. Thiols on gold have been particularly well studied and used as model systems for a variety of applications including biomaterial and biosensor surfaces.[1,2] Recently, octadecyl phosphate has been shown to form adlayers spontaneously from heptane/2-propanol solutions on tantalum oxide ($Ta_2O_5$) surfaces, resulting in highly hydrophobic surfaces with structural and chemical properties resembling those of long-chain alkanethiols on gold.[3,4] In particular, the average tilt angle of 30° (relative to the surface normal) determined by near-edge X-ray absorption fine structure (NEXAFS) spectroscopy and the detection by atomic force microscopy (AFM) of (local) two-dimensional, hexagonal patterns of the terminal methyl group with a characteristic intermolecular spacing of 0.49 nm (measured parallel to the surface) are similar to the corresponding characteristic values reported for gold (111)/alkanethiol SAMs.[1,5] Tantalum oxide was chosen as a substrate in view of its use in transparent, high-refractive-index waveguiding layers in optical sensor applications.[6,7] The production of bioaffinity sensor surfaces with controlled chemical properties is of great relevance in the areas of DNA/RNA and protein sensing, genomics, and proteomics.[8]

The use of organic solvents to produce surface layers has clear disadvantages if the aim is to use such techniques on an industrial scale (due to both environmental emission and disposal issues). Moreover, for applications in areas such as medical devices and implants, the presence of even minor organic solvent residues in the adlayers cannot be tolerated, in view of potential cell-toxicity effects and other biological risks. On the other hand, self-assembled monolayers, in particular of molecules with functional terminal groups, are of great interest for the modification and functionalization of biomaterials and medical devices. Therefore, a technique based on the deposition of SAMs from aqueous alkyl phosphate solutions has been developed and successfully applied to a variety of metal oxide substrates.[9]

This paper covers the deposition and characterization of monolayers of dodecyl phosphate, 12-hydroxy-dodecyl phosphate, and a mixture of the two from aqueous solutions of their ammonium salts onto three different substrates: titanium oxide and titanium metal films, deposited by physical vapor deposition onto glass and silicon substrates (serving as smooth, flat model surfaces), and a special titanium dental implant surface with a rough, highly corrugated surface. The aim of the present investigation is twofold: first, to describe the physicochemical and structural properties of the single-component and mixed SAMs on titanium (oxide), and second, to test the

* To whom correspondence should be addressed.

(1) Bain, C. D.; Troughton, E. B.; Tao, Y. T.; Evall, J.; Whitesides, G. M.; Nuzzo, R. G. *J. Am. Chem. Soc.* **1989**, *111*, 321.
(2) Nuzzo, R.; Allara, D. L. *J. Am. Chem. Soc.* **1983**, *105*, 4481.
(3) Brovelli, D.; Hähner, D.; Ruiz, L.; Hofer, R.; Kraus, G.; Waldner, A.; Schlösser, J.; Oroszlan, P.; Ehrat, M.; Spencer, N. D. *Langmuir* **1999**, *15*, 4324.
(4) Textor, M.; Ruiz, L.; Hofer, R.; Rossi, A.; Feldman, K.; Hähner, G.; Spencer, N. D. *Langmuir* **2000**, *16*, 3257.
(5) Folkers, J. P.; Gorman, C. B.; Laibinis, P. E.; Buchholz, S.; Whitesides, G. M.; Nuzzo, R. G. *Langmuir* **1995**, *11*, 813.
(6) Duveneck, G. L.; Pawlak, M.; Neuschäfer, D.; Bär, E.; Budak, W.; Pieles, U.; Ehrat, M. *Sens. Actuators, B* **1997**, *38*−*39*, 88.
(7) Budach, W.; Abel, A. P.; Bruno, A. E.; Neuschafer, D. *Anal. Chem.* **1999**, *71*, 3347.
(8) Duveneck, G. L.; Abel, A. P. *Proc. SPIE* (*Prepr.*) **1999**, Vol. 3858.
(9) Hofer, R.; Textor, M.; Spencer, N. D. *Langmuir* **2001**, *17*, 4014.

10.1021/la011459p CCC: $22.00 
Published on Web 04/05/2002

feasibility of using alkyl phosphate based SAMs to tailor the surface properties of titanium medical devices.

## 2. Materials and Methods

**2.1. Substrates.** Three different substrates were used. Thin films of titanium dioxide ($TiO_2$) (20 nm thick) and of titanium (Ti(metal)) (100 nm thick) were deposited by physical vapor deposition (PVD, reactive magnetron sputtering, Paul Scherrer Institut, Villigen, Switzerland) onto silicon wafers and flat glass slides, respectively. Before the coating, the uncoated substrates were ultrasonically cleaned in toluene (Uvasol, Merck, Dietikon, Switzerland) for 15 min and dried under flowing nitrogen gas (5.0). Commercially pure titanium (CP Ti) disks, 15 mm in diameter and 1 mm in thickness, were grit-blasted with alumina beads (average particle size, 250 $\mu$m) under low-impact-energy, industrial particle-blasting conditions and subsequently etched in a hot solution of $HCl/H_2SO_4$ (Institut Straumann AG, Waldenburg, Switzerland). This surface, known commercially as "SLA", is characterized by a duplex surface topography with roughness contributions in the range of typically 20−50 $\mu$m (originating from the blasting process) and 0.5−2 $\mu$m (from the chemical etching process).

**2.2. Self-Assembled Monolayers.** Ammonium salts of dodecyl ($DDPO_4$) and 12-hydroxy dodecyl phosphate ($OH-DDPO_4$) were precipitated from a 2-propanol (UVASOL, Merck) solution of the free acid molecules using ammonia (25% aq, p.a., Merck). Details are given in refs 9 and 10. Equimolar solutions (0.5 mM) of both amphiphiles were prepared by dissolving their corresponding ammonium salts in high-purity water (HPLC, Fluka, Buchs, Switzerland) at 50 °C and subsequently cooling to room temperature. The alkyl phosphate and hydroxyalkyl phosphate aqueous solutions were mixed in different ratios from 0:100 to 100:0 vol % in steps of either 10% or 25% with respect to the amount of $OH-DDPO_4$. Cleaning and SAM formation for $TiO_2$ and Ti(metal) samples were carried out according to details given in previous papers.[9,10] The samples were immersed for 48 h in the amphiphile solution and then removed, each being rinsed with 10 mL of high-purity water (HPLC, Fluka) and finally blown dry with nitrogen (5.0 purity).

**2.3. X-ray Photoelectron Spectroscopy (XPS).** XPS spectra were recorded with a SAGE 100 system (Specs, Berlin, Germany) using nonmonochromatized Al Kα radiation at 320 W (13 kV) and an electron-energy analyzer pass energy of 50 eV for low-resolution surveys and of 14 eV for high-resolution detailed scans. The analyzed area was 6 $mm^2$, and the results therefore represent a laterally averaged chemical composition. To determine the quantitative surface composition from XPS data, the sensitivity factors of Scofield[11] are used. All binding energies are referenced relative to the main hydrocarbon peak (from residual contamination in the case of the clean surfaces and the SAM hydrocarbon chain in the case of the SAM-coated surfaces), set at a binding energy of 285.0 eV.

**2.4. Atomic Force Microscopy (AFM).** AFM measurements were performed with a commercial scanning probe microscope (Nanoscope III, Digital Instruments, Santa Barbara, CA). Measurements of surface topography and lateral force were made simultaneously by operating the instrument in contact mode while scanning the cantilever laterally. All measurements were performed in ambient air on freshly plasma cleaned samples.

**2.5. Contact-Angle Measurements.** Surface wettability was investigated by measuring advancing and receding contact angles in a sessile water drop experiment (Contact Angle Measuring System, G2/G40 2.05-D, Krüss GmbH, Hamburg, Germany). The measurements were performed in an automated way by increasing and decreasing the water drop size stepwise. Averaged data and error bars refer to six advancing-angle and three receding-angle measurements at different locations on each sample.

**2.6. Time-of-Flight Secondary Ion Mass Spectrometry (ToF-SIMS) Measurements.** Secondary ion mass spectra were recorded on a PHI 7200 time-of-flight secondary ion mass spectrometer (Physical Electronics, Eden Prairie, MN) in the mass range 0−1000 *m/e*. The total ion dose of the 8 kV $Cs^+$ primary ion beam (100 $\mu$m diameter) was below the static limit ($<1.0 \times 10^{13}$ ions/$cm^{-2}$). Time per data point was 1.25 ns. Three positive and three negative spectra were taken across the sample to ensure reproducibility and determine homogeneity of the monolayers. Mass resolution $M/\Delta M$ was typically around 5000 in the positive and 3000 in the negative mode. The PHI Tofpack software was used to calibrate the entire mass range from a single standard set of low ion masses. To improve the quality of mass calibration in the higher mass range, a higher-mass metal ion peak was used in addition.

**Table 1. Roughness Values $R_a$ and $R_q$ for the Different Substrates**

| substrate | PVD coating | roughness values | |
|---|---|---|---|
| glass | | $R_q$ | 5.65 ± 0.28 nm[a] |
| | | $R_a$ | 3.78 ± 0.19 nm[a] |
| | $TiO_2$ | $R_q$ | 3.63 ± 0.18 nm[a] |
| | | $R_a$ | 2.05 ± 0.10 nm[a] |
| | Ti(metal) | $R_q$ | 3.85 ± 0.19 nm[a] |
| | | $R_a$ | 2.48 ± 0.12 nm[a] |
| Si wafer | | $R_q$ | 0.11 ± 0.01 nm[a] |
| | | $R_a$ | 0.07 ± 0.01 nm[a] |
| | $TiO_2$ | $R_q$ | 0.60 ± 0.03 nm[a] |
| | | $R_a$ | 0.44 ± 0.02 nm[a] |
| | Ti(metal) | $R_q$ | 1.67 ± 0.08 nm[a] |
| | | $R_a$ | 1.32 ± 0.07 nm[a] |
| Ti(metal) | blasted, acid-etched (SLA) | $R_q$ | 2.01 ± 0.22 $\mu$m[b] |
| | | $R_a$ | 2.56 ± 0.28 $\mu$m[b] |

[a] Measured with AFM over a 10 × 10 $\mu$m area and calculated from lines of different scan lengths. [b] Measured with the noncontact laser profilometer technique (ref 12) in a scan range of 10−50 $\mu$m.

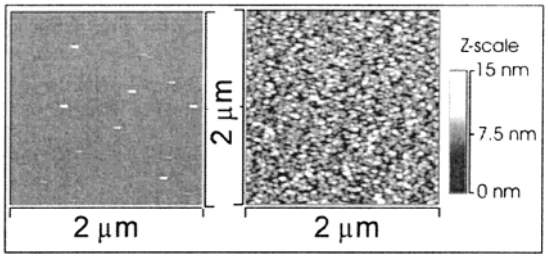


**Figure 1.** AFM images of $TiO_2$ (left) and Ti(metal) (right) on a silicon wafer. Scan area: 2 × 2 $\mu$m.

## 3. Results

**3.1. Properties of the Clean Titanium (Oxide) Surfaces.** The surfaces of all three types of substrates were cleaned according to the protocol given in refs 9 and 10 and characterized by XPS, AFM, and scanning electron microscopy (SEM). Roughness parameters of the different substrates were determined using AFM line scans in characteristic areas along distances of 10, 2, and 0.5 $\mu$m. They are reported as $R_a$ and $R_q$ values in Table 1. In the case of the Si wafer, the titanium oxide surface is very smooth with a roughness that is only slightly higher than that of the wafer substrate surface, while the titanium metal surface is significantly rougher. These findings can be explained by the fact that the PVD-deposited oxide film is amorphous, while the titanium metal film is expected, at least partially, to recrystallize following deposition, inducing grain-size- and grain-orientation-related topographic features at the surface (Figure 1). Roughness measurements on the blasted, acid-etched surface (SLA) were performed using the noncontact laser profilometry technique.[12,13] The roughness parameters are summarized in Table 1. The experimental values are characteristic of the complex topography of alumina-blasted, acid-etched

(10) Hofer, R. Surface Modification for Optical Biosensor Application. Ph.D. Thesis No. 13873, ETH Zürich, Zürich, Switzerland, 2000.

(11) Scofield, J. H. *J. Electron Spectrosc. Relat. Phenom.* **1976**, *8*, 129.

(12) Wieland, M. Ph.D. Thesis No. 13247, ETH Zürich, Zürich, Switzerland, 1999.

**Table 2. XPS Binding Energies ($E_B \pm 0.1$ eV) of the Different Peak Components and Normalized Intensities[a] of Cleaned Titanium Oxide and Titanium Metal Films on Si Wafer Substrates**

| element | assignment | energy [eV] | normalized intensities[a] $TiO_2$ sample | normalized intensities[a] Ti(metal) sample | normalized intensities[a] Ti(SLA) sample |
|---|---|---|---|---|---|
| C(1s)(1) | **C**$H_2$, **C**$H_3$ contamination | 285.0 | 6.9 | 6.4 | 8.8 |
| C(1s)(2) | −**C**−O−H, −**C**−OOH contamination | 286.5, 289.0 | | | |
| O(1s)(1) | Ti**O**$_2$ | 530.1 | 64.3 | 62.0 | 61.9 |
| Ti(2p1/2) | **Ti(metal)** | 454.1 | | 8.3 | 4.6 |
| Ti(2p3/2) | **Ti(metal)** | 459.7 | | | |
| Ti(2p1/2) | **Ti**$O_2$ | 458.7 | 28.8 | 23.3 | 24.7 |
| Ti(2p3/2) | **Ti**$O_2$ | 464.4 | | | |

[a] Experimental (overall) peak areas divided by the corresponding elemental sensitivity factors and expressed as a percentage of the summed normalized peak areas.

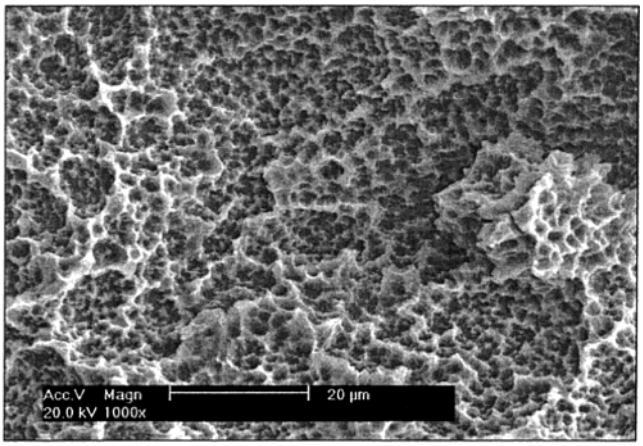


**Figure 2.** SEM image of the topography of the particle-blasted and acid-etched CP titanium (SLA) surface.

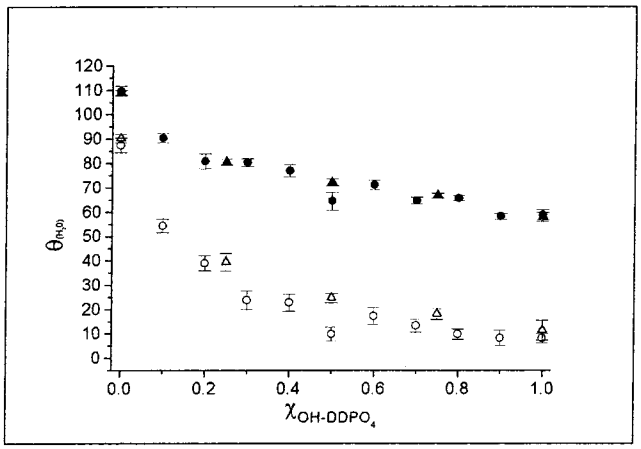


**Figure 3.** Advancing and receding contact angles of water on smooth titanium dioxide coated glass (adv = ●; rec = ○) and silicon wafer (adv = ▲; rec = △) surfaces as a function of the $OH-DDPO_4(NH_4)_2$ concentration in the SAM-forming solution, expressed as a mole fraction, $\chi_{OH-DDPO_4} = [OH-DDPO_4(NH_4)_2]/\{[OH-DDPO_4(NH_4)_2] + [DDPO_4(NH_4)_2]\}$.

titanium surfaces.[12−14] A SEM image of the SLA surface taken at a magnification of 1000 is shown in Figure 2.

The XPS results (Table 2) show the presence of titanium, oxygen, and carbon, as expected for a well-cleaned titanium (oxide) surface.[15] The carbon is due to adventitious contamination that cannot be prevented in practice for samples exposed even briefly to ambient air. However, in our experience, this degree of contamination is low enough not to interfere adversely with the subsequent self-assembly process.

The water contact angles are typically below 10° for the flat titanium oxide and titanium metal surfaces when measured immediately (<5 min) after UV/ozone cleaning.

Positive ion ToF-SIMS spectra of the bare, smooth $TiO_2$ surfaces exhibit peaks resulting from hydrocarbon contamination, including the peak series $C_nH_{2n+1}^+$ and $C_nH_{2n-1}^+$, and from a few further contaminants, such as $NH_4^+$ and $Na^+$, present at very low concentrations (not detectable by XPS). The main peaks, however, are due to mono- or multinuclear oxide species of the general type $Ti_aO_bH_c$, with $Ti^+$ and $TiO^+$ displaying the highest intensities.[4] The negative ion spectra exhibit $O^-$ and $OH^-$ as the most prominent peaks observed from the oxide surface. Smaller peaks due to hydrocarbon contamination and some recombinant $Ti_aO_bC_cH_d$ peaks at higher mass ranges are also detected.[16,17] These data are consistent with results published previously on clean titanium oxide surfaces.[4,15]

**3.2. Formation of Self-Assembled Monolayers and Contact-Angle Measurement.** The alkyl phosphate and hydroxyalkyl phosphate solutions were mixed in different ratios from 0 to 100 vol %, leading to solutions with different mole fractions $\chi_{OH-DDPO_4} = [OH-DDPO_4(NH_4)_2]/\{[OH-DDPO_4(NH_4)_2] + [DDPO_4(NH_4)_2]\}$ at a constant total phosphate concentration of 0.5 mM. Following the protocols given in section 2.2, self-assembled monolayers were prepared on the smooth and structured samples. The water sessile drop contact-angle data are plotted in Figures 3−5 for the three different types of surfaces exposed to the amphiphile solution at different values of $\chi_{OH-DDPO_4}$ for 48 h. The advancing/receding contact angles on the SAM-coated, flat titanium metal and titanium oxide substrates show a relatively smooth, continuous change from around 110°/85° for the pure methyl-terminated SAM to around 55°/10° for the pure hydroxy-terminated SAM layers, with a clear trend toward increasing hysteresis (difference between advancing and receding angles) as the $OH-DDPO_4$ content ($\chi_{OH-DDPO_4}$) of the SAM solution is increased. The corresponding experimental data for the rough SLA surface, on the other hand, are quite different, with comparatively much higher advancing contact angles of between ca. 150° ($DDPO_4$) and 100° ($OH-DDPO_4$) being

(13) Wieland, M.; Textor, M. Measurement and Evaluation of the Chemical Composition and Topography of Titanium Implant Surfaces. In *Bone Engineering*; Davies, J. E., Ed.; em squared: Toronto, 2000; pp 163−182.

(14) Vörös, J.; Wieland, M.; Ruiz-Taylor, L.; Textor, M.; Brunette, D. M. Characterization of Titanium Surfaces. In *Titanium in Medicine*: *Material Science, Surface Science, Engineering, Biological Responses and Medical Applications*; Springer-Verlag: Berlin, 2001; pp 87−144.

(15) Textor, M.; Sittig, C.; Frauchiger, V.; Tosatti, S.; Brunette, D. M. Properties and Biological Significance of Natural Oxide Films on Titanium and Its Alloys. In *Titanium in Medicine*: *Material Science, Surface Science, Engineering, Biological Responses and Medical Applications*; Springer-Verlag: Berlin, 2001; pp 171−230.

(16) Lazzeri, P.; Lui, A.; Moro, L.; Vanzetti, L. *Surf. Interface Anal.* **2000**, *29* (11), 798.

(17) Michiels, F.; Adams, J. *Anal. At. Spectrosc.* **1987**, *2* (8), 773.

**Table 3. XPS Binding Energies ($E_B \pm 0.1$ eV) of the Different Peak Components and Normalized Intensities of the Smooth Titanium Oxide ($TiO_2$ on Glass) Surface Covered with Self-Assembled Monolayers of Methyl- or Hydroxy-Terminated Dodecyl Phosphate**

| element | assignment | energy [eV] | normalized intensities $I'$ [a] $DDPO_4$ SAM | normalized intensities $I'$ [a] $OH-DDPO_4$ SAM |
|---|---|---|---|---|
| C(1s)(1) | **C**$H_2$, **C**$H_3$ | 285.0 | 27.0 | 29.3 |
| C(1s)(2) | **C**−O−P, **C**−O−H (only $OH-DDPO_4$) | 286.5 | | |
| O(1s)(1) | Ti**O**$_2$ | 530.1 | 50.2 | 49.4 |
| O(1s)(2) | Ti−**O**−P, P=**O** | 531.3 | | |
| O(1s)(3) | P−**O**−H, P−**O**−R | 532.6 | | |
| O(1s)(4) | C−**O**−H (only $OH-DDPO_4$) | 533.4 | | |
| P(2p) | C−O−**P**(=O)$(O^-)_2$ | 134.0 | 2.5 | 2.5 |
| Ti(2p1/2) | **Ti**$O_2$ | 458.7 | 20.3 | 18.8 |
| Ti(2p3/2) | **Ti**$O_2$ | 464.4 | | |

[a] Experimental (overall) peak areas divided by the corresponding elemental Scofield sensitivity factors.

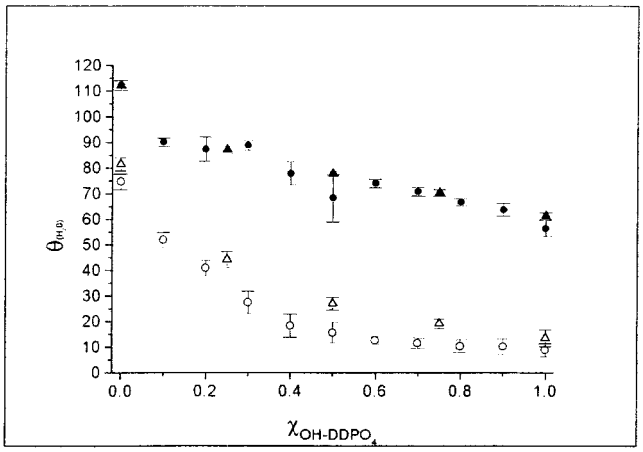


**Figure 4.** Advancing and receding contact angles of water on smooth titanium metal coated glass (adv = ●; rec = ○) and silicon wafer (adv = ▲; rec = △) surfaces as a function of the $OH-DDPO_4(NH_4)_2$ concentration in the SAM-forming solution, expressed as a mole fraction, $\chi_{OH-DDPO_4} = [OH-DDPO_4(NH_4)_2]/\{[OH-DDPO_4(NH_4)_2] + [DDPO_4(NH_4)_2]\}$.

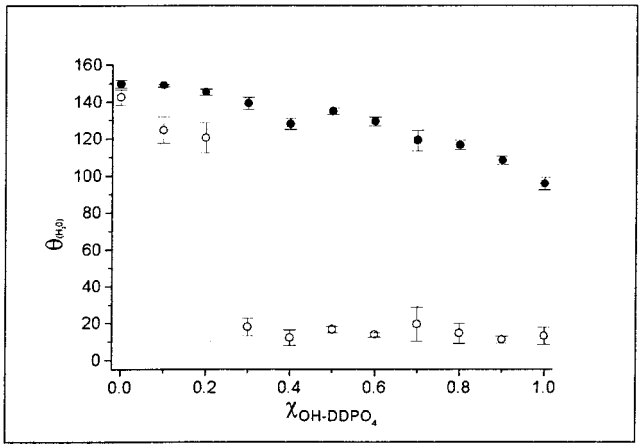


**Figure 5.** Advancing (●) and receding (○) contact angles of water on rough, particle-blasted and acid-etched (SLA) titanium metal surfaces as a function of the $OH-DDPO_4(NH_4)_2$ concentration in the SAM-forming solution, expressed as a mole fraction, $\chi_{OH-DDPO_4} = [OH-DDPO_4(NH_4)_2]/\{[OH-DDPO_4(NH_4)_2] + [DDPO_4(NH_4)_2]\}$.

observed, as well as a characteristic sharp drop in the receding angle at $\chi_{OH-DDPO_4}$ values of 0.2−0.3 and a strong increase in hysteresis for $\chi_{OH-DDPO_4} = 0.3$.

**3.3. XPS Analysis of the SAM-Treated Surfaces.** Table 3 summarizes the experimental binding energies of the C(1s), O(1s), P(2p), and Ti(2p) XPS peaks for a smooth ($TiO_2$ on glass) surface. The peak fitting (deconvolution) of the C(1s) and O(1s) peaks and assignment to particular species were performed according to protocols and argumentation discussed in detail in reference 4. Table 3 also contains the normalized intensities, that is, the experimental intensities (peak areas) divided by the corresponding sensitivity factors and expressed as percentages of the summed normalized peak areas. We deliberately refer to these values as normalized intensities rather than atomic concentrations to make clear that the type of surfaces under investigation should not be treated quantitatively using a homogeneous surface model, that is, assuming that the elemental concentrations are uniformly distributed across the sampling depth of the XPS method. Nevertheless, the data are useful for drawing some general conclusions and for semiquantitative comparisons of the different clean and modified surfaces.

Table 4 lists in detail the position, full width at half-maximum intensity (fwhm), and relative peak areas of the deconvolved C(1s) and O(1s) signals for both the smooth titanium oxide and smooth titanium metal surfaces treated in solutions with $\chi_{OH-DDPO_4} = 0$, 0.5, and 1.0. In Figures 6 and 7, the intensity ratios of C(1s)/Ti(2p), O(1s)/Ti(2p), C(1s)/O(1s), and P(2p)/C(1s) are plotted as a function of $\chi_{OH-DDPO_4}$.

There are relatively minor changes in the intensity ratios (Figures 6 and 7) across the range of $\chi_{OH-DDPO_4}$ values, pointing to relatively constant densities of the assembled molecules independent of the $\chi_{OH-DDPO_4}$ ratio. There seems to be a slight tendency for the C/Ti ratio to increase with increasing $\chi_{OH-DDPO_4}$. Considering the error bars, however, this is not statistically relevant. Two observations are clearly significant: first, the proportion of C−O−R (R = H or C) increases with increasing $\chi_{OH-DDPO_4}$ (Table 4), pointing to an increase of the fraction of $OH-DDPO_4$ in the adlayer, as expected from the contact-angle measurements; second, the C/Ti intensity ratio is much higher in the case of the rough SLA titanium surface in comparison to the flat case (titanium metal or titanium oxide). This is consistent with expectations, since on average the electrons have to travel a longer distance through the SAM layer for a rough surface with a mean angle of inclination, α (relative to the surface plane), that is different from zero (see discussion section). The C(1s) intensity is expected to increase, while the Ti(2p) and O(1s) (oxide) intensities decrease with increasing α, making the C(1s)/Ti(2p) ratio a sensitive measure of the average tilt angle, α, of the surface. Corresponding quantitative analysis will be presented in the discussion section.

**3.4. ToF-SIMS of SAM Surfaces.** For the series of mixed self-assembled monolayer surfaces ($\chi_{OH-DDPO_4} = 0$, 0.25, 0.5, 0.75, 1), two negative ion spectra per sample were recorded for three independent series. The dodecyl phosphate molecular ion peak, with the loss of one hydrogen $(M - H)^-$ in the negative secondary ion spectrum,

**Table 4. Differences in the XPS Binding Energies ($E_B \pm 0.1$ eV), Full Widths at Half-Maximum, and Relative Peak Areas of Oxygen and Carbon Peaks after Curve Fitting for SAMs Assembled from Solutions with Different Molar Fractions, $\chi_{OH-DDPO_4}$[a]**

| | | | | relative element areas for $\chi_{OH-DDPO_4} = 0$ | | | relative element areas for $\chi_{OH-DDPO_4} = 0.5$ | | | relative element areas for $\chi_{OH-DDPO_4} = 1$ | | |
|---|---|---|---|---|---|---|---|---|---|---|---|---|
| peak | species | $\Delta E^b$ [eV] | fwhm | calc | expt $TiO_2$ | expt Ti(metal) | calc | expt $TiO_2$ | expt Ti(metal) | calc | expt $TiO_2$ | expt Ti(metal) |
| C(1s)(1) | $CH_2$, $CH_3$ | | 1.55 | 90.9 | 91.4 | 89.0 | 86.4 | 85.0 | 85.9 | 81.8 | 82.2 | 81.5 |
| C(1s)(2) | C−O−P, C−O−H | 1.60 | 1.75 | 9.1 | 8.6 | 10.9 | 13.6 | 15.0 | 14.1 | 18.2 | 17.8 | 18.5 |
| O(1s)(1) | $TiO_2$ | | 1.55 | | 79.5 | 70.1 | | 76.1 | 69.4 | | 73.9 | 67.7 |
| O(1s)(2) | Ti−O−P, P═O | 1.25 | 1.70 | | 15.6 | 22.4 | | 14.9 | 20.2 | | 15.8 | 19.3 |
| O(1s)(3) | P−O−H, P−O−R | 2.55 | 1.70 | | 4.9 | 7.5 | | 6.3 | 8.4 | | 5.0 | 8.9 |
| O(1s)(4) | C−O−H | 3.35 | 1.70 | | | | | 2.7 | 2.0 | | 5.3 | 4.1 |

[a] Substrates: titanium oxide and titanium metal coatings on silicon substrates. [b] Binding energy shift relative to main peak component.

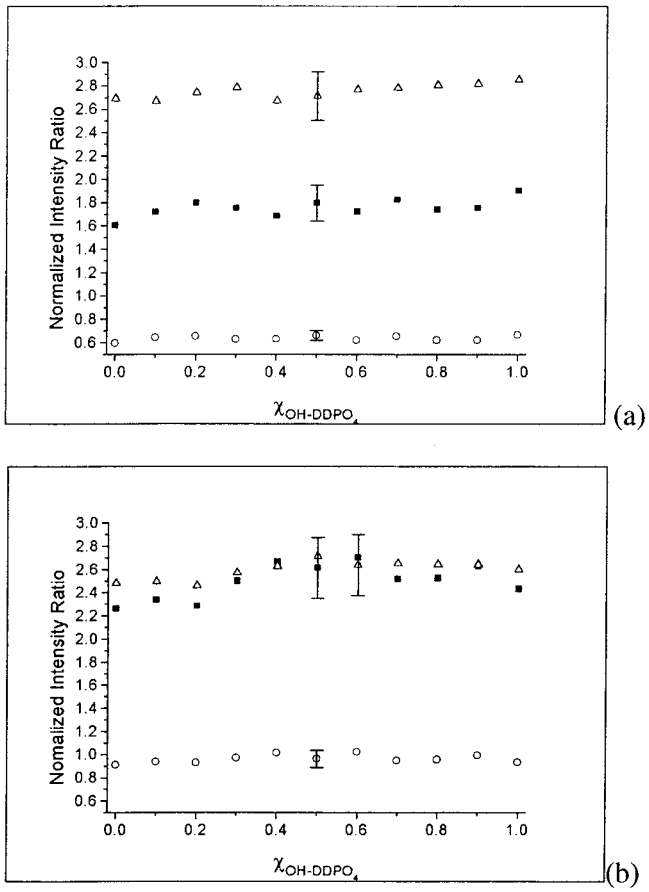


**Figure 6.** XPS normalized intensity ratios C/Ti (■), C/O (○), and O/Ti (△) for the smooth titanium oxide on glass (a) and rough (SLA) titanium (b), after SAM formation in solutions of different molar fractions, $\chi_{OH-DDPO_4} = [OH-DDPO_4(NH_4)_2]/\{[OH-DDPO_4(NH_4)_2] + [DDPO_4(NH_4)_2]\}$.

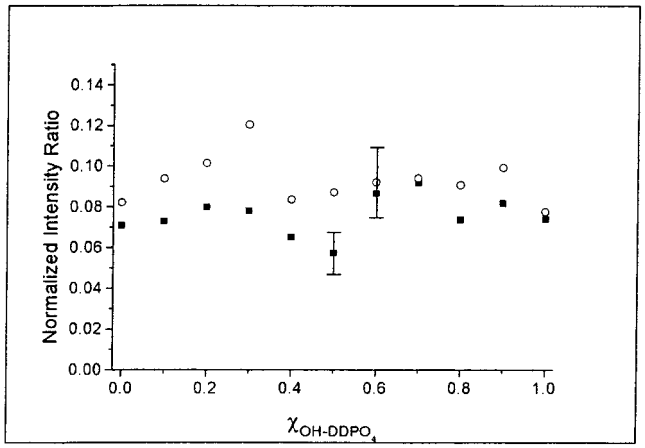


**Figure 7.** XPS normalized intensity ratios P/C on the smooth titanium oxide surface ($TiO_2$ on glass) (■) and the rough (SLA) titanium metal (○) surface, after SAM formation in solutions of different molar fractions, $\chi_{OH-DDPO_4} = [OH-DDPO_4(NH_4)_2]/\{[OH-DDPO_4(NH_4)_2] + [DDPO_4(NH_4)_2]\}$.

was used to semiquantitatively evaluate the composition of the pure and mixed alkane phosphate adlayers. The comparison between the spectra of the clean $TiO_2$ surface and the $DDPO_4$ monolayer is in good agreement with the results of a previous study,[4] which described the adsorption of octadecyl phosphate onto $Ta_2O_5$ surfaces.

In general, SIMS cannot be considered a quantitative analytical technique due to strong matrix effects on secondary ion intensities.[16−18] However, under favorable conditions, for example, when a series of closely chemically related samples are measured under the same experimental conditions, *semi*quantitative results can be achieved.[19,20] We used sets of SAM samples that were prepared according to the same protocol and measured using the same experimental parameters. In the *positive* ion mode, the $DDPO_4$ self-assembled surface displays similar hydrocarbon ion peaks to that of the bare oxide (in this case due to adventitious hydrocarbon contamination), but with strongly decreased contaminant peak intensity ($Na^+$, $NH_4^+$, etc.), as well as decreased intensities of the $Ti^+$ and $TiO^+$ peaks. Fragments of the type $C_aH_bP_cO_d$, $Ti_aP_bO_cH_d$, and $Ti_aP_bO_cC_dH_e$ are indicative of the formation of a SAM and of a direct bond between the phosphate headgroup and the metal cations at the oxide surface. The *negative* ion spectra displayed strong $PO_2^-$ and $PO_3^-$ fragments that were not observed on the clean surfaces, as well as the molecular mass peaks $(M - H)^-$ characteristic of the two types of alkane phosphates ($DDPO_4$ at 265.16, $OH-DDPO_4$ at 281.15), providing good evidence that alkane phosphate molecules chemisorb in molecular form (i.e., without decomposition) onto the $TiO_2$ surface.

The molecular ion $(M - H)^-$ intensity of the methyl-terminated phosphate is 1 order of magnitude greater than that of the hydroxy-terminated phosphate. It has been reported that the detection of molecular mass ions M − H is correlated with the degree of order in self-assembled monolayers, resulting from energy transfer and stability effects.[21] We assume that the higher count rate

(18) Vickerman, J. C.; Brown, A.; Reed, N. *Secondary ion mass spectrometry*: *principles and applications*; Clarendon Press: Oxford, 1989.

(19) Chakraborty, P. *Pramana* **1998**, *50* (6), 617.

(20) Thompson, P. M. *Anal. Chem.* **1991**, *63* (21), 2447.

(21) Graham, D. J.; Ratner, B. D. Multivariate Analysis of TOF-SIMS Spectra from Dodecanethiol SAM Assembly on Gold: Spectral interpretation and TOF-SIMS fragmentation processes. *Langmuir*, submitted.

**Table 5. Thicknesses of the Different Layers Used for Quantitative XPS-Based Calculations Assuming the Model of Figure 9 with an Ordered SAM and Molecular Tilt Angle of 30° Relative to the Surface Normal**

| layer no. | chemistry | atom code[a] | parameter code | thickness[b] [nm] for SAM on $TiO_2$ surface | thickness[b] [nm] for SAM on Ti(metal) surface |
|---|---|---|---|---|---|
| 1 | Ti(metal) | Ti(metal) | $d_{Ti(metal)}$ | | semi-infinite |
| 2 | $TiO_2$ | $TiO_2$ or O1 | $d_{TiO_2}$ | semi-infinite | 5.0[c] |
| 3 | phosphate group | P, O2, O3 | $d_{PO_4}$ | 0.37 | 0.37 |
| 4 | carbon chain for $DDPO_4$ and OH-$DDPO_4$ | C1, C2 | $d_{(CH_2)12}$ | 1.3 | 1.3 |
| 5 | hydroxy group (OH, only OH-$DDPO_4$) | O4 | $d_{OH}$ | 0.11 | 0.11 |

[a] See Table 4. [b] Measured perpendicular to the surface plane. [c] Natural oxide film thickness calculated from XPS intensity ratio $I$(Ti(2p), oxide)/$I$(Ti(2p), metal) of a clean surface (see text).

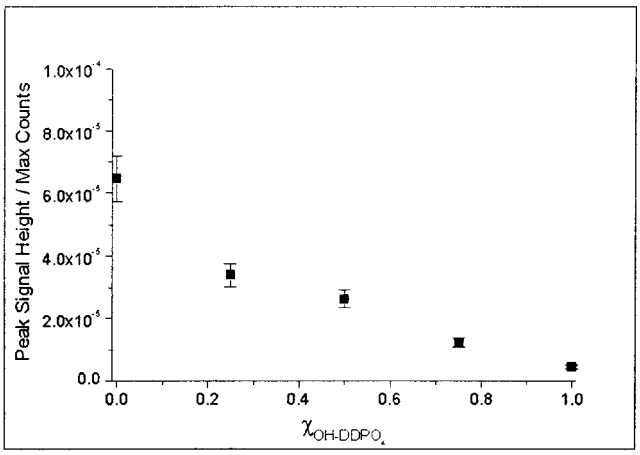


**Figure 8.** ToF-SIMS normalized peak signal heights of the $DDPO_4$ negative ion $(M - H)^-$ on smooth titanium oxide surfaces ($TiO_2$ on Si wafer) (■) after SAM formation in solutions of different molar fractions, $\chi_{OH-DDPO_4} = [OH-DDPO_4(NH_4)_2]/\{[OH-DDPO_4(NH_4)_2] + [DDPO_4(NH_4)_2]\}$.

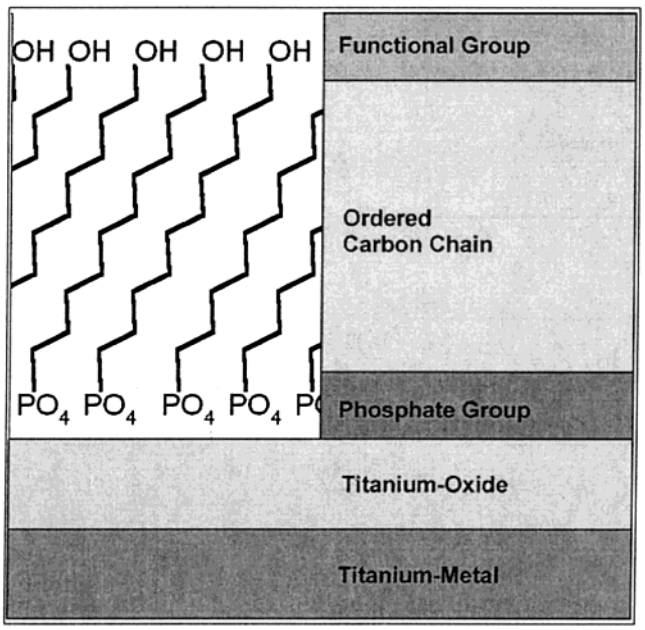


**Figure 9.** Idealized view and structural model of the alkane phosphate SAM on the titanium/titanium oxide substrate.

of the methyl-terminated phosphate is due to higher order in the self-assembled monolayer as well as to lower cohesion effects that may hinder the desorption of a hydrogen-bonded network of hydroxyl-terminated phosphates.

Therefore, the methyl-terminated phosphate signal can be used to show the dependency of the surface composition of the mixed self-assembled monolayers on the molar concentrations of the amphiphile in solution. Figure 8 shows the relative counts for the $DDPO_4$ ion expressed as a function of the solution molar fraction of the OH-terminated molecule ($\chi_{OH-DDPO_4}$). If taken quantitatively, this would represent a nonlinear dependence similar to the observations based on our other measurement techniques and in that way supports our view of the dependence of adlayer composition on assembly solution composition. However, it has to be admitted that the situation is rather complex in the sense that the adlayer composition and order are changing at the same time. More information on the order of these mixed adlayers is presented elsewhere.[22]

**3.5. Model Calculations Based on XPS Results.** This section concerns a multilayer model for the SAM-covered surface and corresponding calculations of XPS intensities based on standard equations and depending on the molecular orientation and packing density within the adlayer. The calculations are first applied to the less complex, smooth surfaces and then to the rough (SLA) case.

**3.5.1. Smooth Case.** *Model.* Based on earlier studies of molecular order and orientation in alkane phosphate SAMs on metal oxide surfaces,[4,9,10] a model assuming a uniform, dense packing of molecules tilted by an angle of 30° to the surface normal was used (Figure 9).

Based on this idealized model and using standard bond lengths,[23] the thicknesses of the different layers were estimated (Table 5). These layer thicknesses are used as input parameters for the calculations discussed below.

The following standard formulas for the intensity of the various photoelectron peaks were used:

Layer 1:

$$I^{Ti}_{Ti(metal)} \propto n^{Ti}_{Ti(metal)}\,\sigma_{Ti}\,T_{Ti}\,\lambda^{Ti}_{Ti(metal)}\exp\left(\frac{-d_{SAM+Oxide}}{\lambda^{Ti}_{SAM+Oxide}\sin(\Theta)}\right) \quad (1)$$

Layer 2:

Natural $TiO_2$ layer for Ti(metal) surfaces:

$$I^{Ti}_{TiO_2;Natural-Oxide} \propto n^{Ti}_{TiO_2}\,\sigma_{Ti}\,T_{Ti}\,\lambda^{Ti}_{TiO_2}\exp\left(\frac{-d_{SAM}}{\lambda^{Ti}_{SAM}\sin(\Theta)}\right)\times\left(1-\exp\left(\frac{-d_{TiO_2}}{\lambda^{Ti}_{TiO_2}\sin(\Theta)}\right)\right) \quad (2)$$

(22) Zwahlen, M.; Tosatti, S.; Textor, M.; Hähner, G. *Langmuir*, in press.

(23) *CRC Handbook of Chemistry and Physics* (*1913−1995*), 75th ed.; Lide, D. R., Ed.; CRC Press: Boca Raton, FL, 1994.

**Table 6. Equations Used for the Calculation of the C(1s)/Ti(2p) Ratio for $DDPO_4$ and $OH-DDPO_4$ SAMs on Smooth $TiO_2$ and on Ti(metal) Surfaces Covered by a Natural Oxide Film**

| substrate | $DDPO_4$ SAM | | $OH-DDPO_4$ SAM | |
|---|---|---|---|---|
| $TiO_2$ | $\frac{I^{C}_{DDPO_4}}{I^{Ti}_{TiO_2}}$ | (6) | $\frac{I^{C}_{OH-DDPO_4}}{I^{Ti}_{TiO_2}}$ | (7) |
| Ti(metal) | $\frac{I^{C}_{DDPO_4}}{I^{Ti}_{TiO_2;Natural-Oxide} + I^{Ti}_{Ti(metal)}}$ | (8) | $\frac{I^{C}_{OH-DDPO_4}}{I^{Ti}_{TiO_2;Natural-Oxide} + I^{Ti}_{Ti(metal)}}$ | (9) |

PVD $TiO_2$ layer for $TiO_2$ surfaces:

$$I^{Ti}_{TiO_2} \propto n^{Ti}_{TiO_2}\,\sigma_{Ti}\,T_{Ti}\,\lambda^{Ti}_{TiO_2}\exp\left(\frac{-d_{SAM}}{\lambda^{Ti}_{SAM}\sin(\Theta)}\right) \quad (3)$$

Layer 4:

$$I^{C}_{DDPO_4} \propto n^{C}_{Layer4}\,\sigma_{C}\,T_{C}\,\lambda^{C}_{SAM}\left(1-\exp\left(\frac{-d_{(CH_2)12}}{\lambda^{C}_{SAM}\sin(\Theta)}\right)\right) \quad (4)$$

Layer 5:

$$I^{C}_{OH-DDPO_4} \propto n^{C}_{Layer4}\,\sigma_{C}\,T_{C}\,\lambda^{C}_{SAM}\exp\left(\frac{-d_{OH}}{\lambda^{C}_{SAM}\sin(\Theta)}\right)\times\left(1-\exp\left(\frac{-d_{(CH_2)12}}{\lambda^{C}_{SAM}\sin(\Theta)}\right)\right) \quad (5)$$

Definitions of the variables are presented in Table 7. The ratios were calculated by combining eqs 1−5 in an appropriate manner for each case (Table 6).

Several parameters are needed to estimate the corresponding XPS intensity ratios of eqs 1−9 within our model and to compare them to the experimental observations:

(1) The electron attenuation length (mean free path length $\lambda$) in the various layers was calculated using the general expressions given by Seah:[24]

Organic layer: $$\lambda = B\sqrt{E_{kin}} \quad (10a)$$

$TiO_2$ and Ti(metal) layer:

$$\lambda = \frac{E}{E_p\left[\beta\ln(\gamma E) - \frac{C}{E} + \frac{D}{E}\right]} \quad (10b)$$

with $B = 0.087$ and $E$ = electron energy; for $E_p$, $\gamma$, $C$, and $D$, see eqs 5.23 and 5.24 of ref 24.

(2) The thickness $d_{TiO_2}$ of the oxide film was calculated using eq 11:[25]

$$d_{TiO_2} = \lambda^{Ti}_{TiO_2}\cos(\theta)\ln\left(\frac{I^{Ti}_{TiO_2}}{I^{Ti}_{Ti(metal)}}\,\frac{n^{Ti}_{Ti(metal)}\,\lambda^{Ti}_{(metal)t}}{n^{Ti}_{TiO_2}\,\lambda^{Ti}_{TiO_2}} + 1\right) \quad (11)$$

(3) Atomic densities, $n$, for the titanium oxide and titanium metals were taken from ref 23.

(4) Photoelectron cross sections, $\sigma$, were taken from tabulations published by Scofield.[11]

(5) The density of alkane phosphate molecules at the surface and carbon atoms in layer 4 was calculated assuming a hexagonal arrangement of the molecules in the SAM layer with an intermolecular distance (parallel to the surface) of 0.49 nm as has been reported for octadecyl phosphate SAMs on tantalum oxide.[4] Such a layer has a molecular density of $4.8 \times 10^{14}$ molecules/cm$^2$ and a carbon atomic density of $n^{C}_{Layer4} = 4.5 \times 10^{22}$ atoms/cm$^3$, calculated according to eq 12:

$$n^{C}_{Layer4} = \frac{n^{SAM-molecules}_{Surface}\,N^{C}_{SAM-molecule}}{d_{Layer4}} \quad (12)$$

The parameters and values used as input data for the calculations are summarized in Table 7.

The result of the calculation is the ratio between the C(1s) peak intensity of the alkane chains in the SAM and the Ti(2p) peak intensity of the $TiO_2$ or Ti(metal) substrate. To correct for a small contribution from hydrocarbon contamination, the C(1s) signal intensities (peak areas) of the SAM samples have been reduced by 7.5%, a value deduced from the XPS spectra of the corresponding bare (cleaned) titanium (oxide) surfaces.

The results of the experimental and calculated C(1s)/Ti(2p) intensity ratios are plotted in Figure 10 for the mixed SAMs (a) on the smooth $TiO_2$ and (b) on the smooth Ti(metal) substrate as a function of the solution molar fraction, $\chi_{OH-DDPO_4}$.

Figure 10 demonstrates that the agreement between the experimental ratios and the corresponding calculated values is quite satisfactory, in view of the experimental uncertainty (the C(1s)/Ti(2p) intensity ratio is a parameter that is highly sensitive to variations in SAM film thickness or density) and in view of the crude approximations of parameters such as $\lambda$. Two conclusions can be drawn. First, the density of the self-assembled molecules at the two titanium (oxide) surfaces appears to be comparable to that found experimentally for octadecyl phosphate on tantalum oxide as evidenced by the fairly good agreement between experimental and theoretical data based on the assumption of the same molecular density in both cases. Second, there seems to be no statistically significant trend for changes in the density of the organophosphate molecules (or of the effective adlayer thickness) within the SAM as one moves from the pure $DDPO_4$ SAM through the mixed adlayer case to the pure $OH-DDPO_4$ SAM.

The generally observed higher C/Ti ratios for the $OH-DDPO_4$ in comparison to the $DDPO_4$ SAM is likely to be related to one or both of two factors: First, the increase in surface energy that accompanies the increase in OH surface density is likely to increase the susceptibility to hydrocarbon surface contamination.[26] Second, differences in the structural order of the adlayer can also decrease the resistance of the surface to recontamination.[21] Such small differences in molecular order probably remain undetected by XPS but seem to affect the results of other techniques, such as ToF-SIMS.

(24) *Practical Surface Analysis*, 2nd ed.; Briggs, D., Seah, M. P., Eds.; John Wiley & Sons: New York, 1990; Vol. 1, Chapter 5.

(25) Sittig, C. E. Ph.D. Thesis No. 12657, ETH Zürich, Zürich, Switzerland, 1998.

(26) Barthlott, W.; Neinhuis, C. *Planta* **1997**, *202*, 1.

**Table 7. List of Parameters, Definitions, and Values Used for the Calculations of XPS Intensity Ratios (Equations 1−9) within the Model**

| parameter | description | value |
|---|---|---|
| $n^{Ti}_{TiO_2}$ | titanium atom density in $TiO_2$ | $2.9 \times 10^{22}$ atoms/cm$^3$ |
| $n^{Ti}_{Ti(metal)}$ | titanium atom density in Ti(metal) | $5.6 \times 10^{22}$ atoms/cm$^3$ |
| $\lambda^{Ti}_{TiO_2}$ | electron attenuation length of Ti(2p) in $TiO_2$ | 1.86 nm |
| $\lambda^{Ti}_{Ti(metal)}$ | electron attenuation length of Ti(2p) in Ti(metal) | 2.11 nm |
| $\lambda^{Ti}_{SAM}$ | electron attenuation length of Ti(2p) in the organic adlayer | 2.75 nm |
| $\lambda^{C}_{SAM}$ | electron attenuation length of C(1s) in the organic adlayer | 3.32 nm |
| $\lambda^{Ti}_{SAM+Oxide} = X_{SAM}\lambda^{Ti}_{SAM} + X_{TiO_2}\lambda^{Ti}_{TiO_2}$ where $X_i$ = fractional layer $i$ with $X_{SAM} + X_{TiO_2} = 1$ | electron attenuation length of Ti(2p) through the oxide film and the organic adlayer | 2.08 nm |
| $\sigma_C$ | C(1s) photoelectron cross section | 1 |
| $\sigma_{Ti}$ | Ti(2p) photoelectron cross section | 7.81 |
| $\Theta$ | takeoff angle relative to the surface plane | 90° |

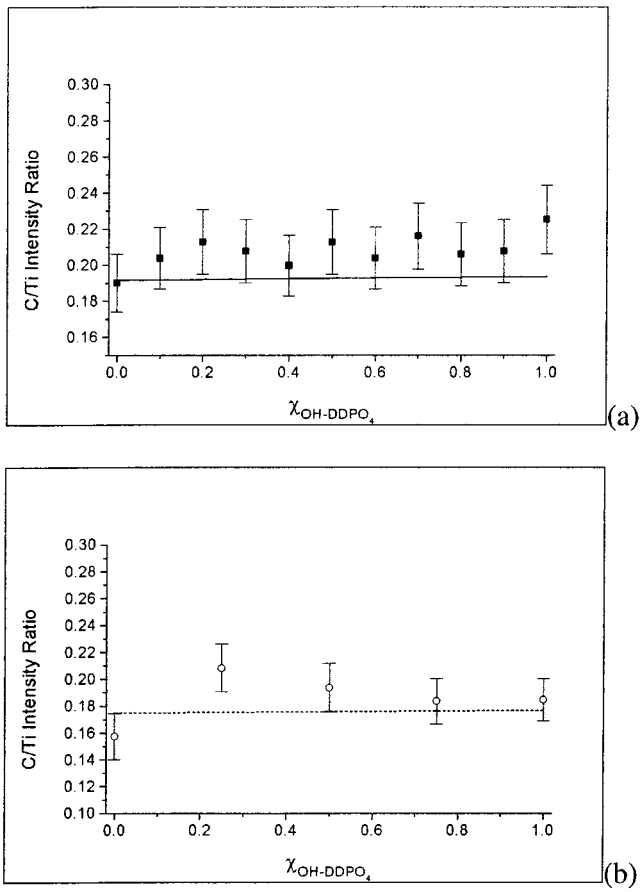


**Figure 10.** C(1s)/Ti(2p) XPS intensity ratios as a function of the composition of the self-assembly solution, $\chi_{OH-DDPO_4} = [OH-DDPO_4(NH_4)_2]/\{[OH-DDPO_4(NH_4)_2] + [DDPO_4(NH_4)_2]\}$, on smooth $TiO_2$ (a) and Ti(metal) (b) on Si wafers. Experimental values are given as symbols together with the estimated error range. The line refers to the calculated ratios assuming a density of $4.8 \times 10^{14}$ molecules/cm$^2$ in the SAM layer, corresponding to a hexagonal close-packed SAM at an intermolecular distance of 0.49 nm (see text).

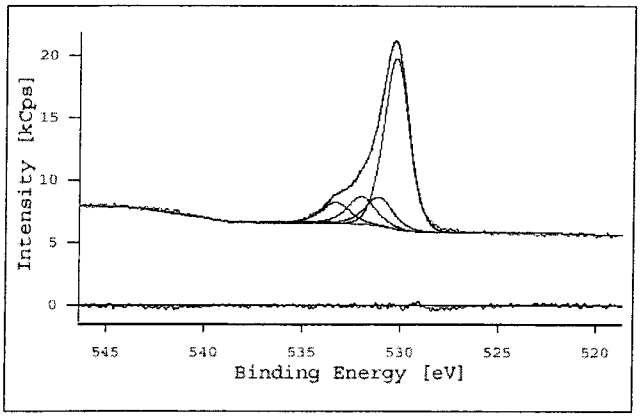


**Figure 11.** XPS oxygen peak (O(1s)) and resolved contributions of O1−O4 (see text), determined for a $OH-DDPO_4$ adlayer on $TiO_2$.

One question remains unanswered at this point: how does the molecular composition of the SAM layer compare with that of the amphiphile solution from which the SAMs have been produced? XPS offers the possibility to deconvolute signals that are characteristic for the $OH-DDPO_4$ molecule and which may be used to quantitatively determine the ratio of $OH-DDPO_4/DDPO_4$ within the organophosphate film. Two different peak components were employed for this purpose: the O(1s) signal of the −C−O−H terminal group (O4) with a binding energy of 533.4 ± 0.1 eV and the C(1s) signal of the same group with a binding energy of 286.5 ± 0.1 eV. In the first case, the hydroxy (O4) component was directly used to calculate the surface concentration of $OH-DDPO_4$. In the second case, the C(1s) binding energy (C2) of −C−O−H is very close (or identical) to that of −C−O−P−. Taking the difference of the C2 peak area between the pure $DDPO_4$ SAM and the mixed SAM therefore eliminated the latter contribution, which was present in the spectra of both $DDPO_4$ and $OH-DDPO_4$. Within a series of samples, the normalized intensity of COH ($I'_{COH}$) was normalized to the total concentration of C atoms (C1 + C2) in order to account for potential instrumental variations (such as X-ray flux) by using eq 13:

$$I'_{COH} = I'_{C2} - \left(\frac{I^{DDPO_4}_{COH}}{I^{DDPO_4}_{C-total}}\right) I'_{C-total} \qquad (13)$$

Figure 11 shows the O(1s) spectrum of the pure $OH-DDPO_4$ SAM on the $TiO_2$ surface together with the resolved contributions from the different oxygen (O1−O4) species present (see also Table 4).

In Figure 12, the normalized concentration of the COH terminal groups relative to the sum of all other C atoms is plotted as a function of the mole fraction, $\chi_{OH-DDPO_4}$.

We conclude from Figure 12 that there are statistical uncertainties when estimating the surface concentration of the terminal C−O−H group as a function of $\chi_{OH-DDPO_4}$. However, it is also obvious that the relationship is not a simple linear one, and a trend toward an increased proportion of $HO-DDPO_4$ in the surface layer in comparison to the solution concentration can be observed,

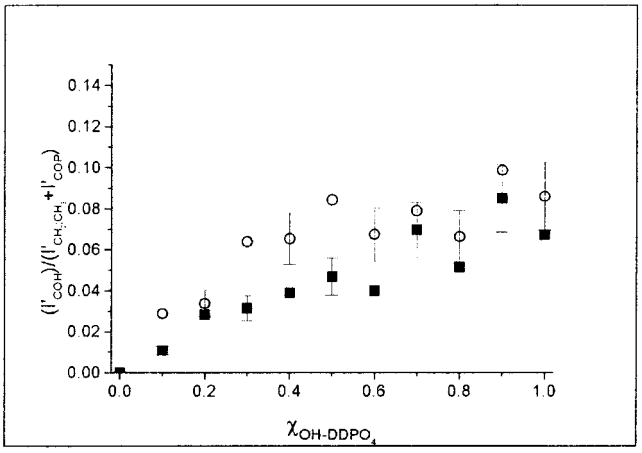


**Figure 12.** Ratio of the normalized intensity COH/(COH + $CH_2$ + $CH_3$ + COP) as a function of $\chi_{OH-DDPO_4}$ calculated from the resolved O(1s) peak contribution C−*O*−H (O4) (■) and the resolved C(1s) peak contribution *C*−O−H (○).

pointing to a preferential adsorption of HO−$DDPO_4$. This will be further discussed in section 4 together with information from contact-angle measurements.

**3.5.2. Rough Surface.** The XPS intensity ratios C(1s)/Ti(2p) for the SAM-coated, rough titanium metal surfaces (SLA) are significantly higher than on the flat titanium (oxide) surfaces. This is to be expected, since the effective local photoelectron takeoff angle is quite different from 90° on a highly rough, high-aspect-ratio surface, such as SLA. Correspondingly, the calculation procedure has to be adapted to account for the topographical effects. The most simple correction procedure was chosen by applying the same formulas as discussed for the flat case but introducing an effective takeoff angle corresponding to an idealized representation of the SLA surface with a single value for the local slope of the surface (Figure 13).

Using eq 11, the effective path length, $d_{TiO_2(SLA)}$, through the oxide layer at an angle of 90° relative to the macroscopic surface plane was calculated to be 6.35 nm. Assuming a 5.0 nm natural oxide layer for CP Ti samples,[25] the effective takeoff angle, α, calculated with the help of eq 14 corresponds to 51.9°.

$$\alpha = \frac{\pi}{2} - \arccos\left(\frac{d_{TiO_2(flat)}}{d_{TiO_2(SLA)}}\right) \qquad (14)$$

The intensity ratios, C(1s)/Ti(2p), were now calculated again using eqs 1, 2−12 but replacing the thickness, *d*, of each surface layer by the effective path length $d' = d/\cos[(\pi/2) - \alpha]$. Within the experimental uncertainty, the experimental C(1s)/Ti(2p) intensity ratios agree with the calculated curve (Figure 14).

## 4. Discussion

**4.1. Formation and Properties of Organophosphate SAMs on Smooth Surfaces.** The combined results of XPS, ToF-SIMS, and contact-angle investigations provide good evidence for the formation of spontaneously formed monomolecular adlayers of dodecyl phosphate ($DDPO_4$) and hydroxy-terminated dodecyl phosphate (OH−$DDPO_4$) on titanium oxide, as well as on titanium metal coated glass and silicon substrates. The oxide and metal substrate surfaces behave similarly in terms of the properties of the SAMs, which is to be expected, since on the metallized surface the outermost layer of ca. 4−5 nm is composed of an amorphous, naturally formed oxide.

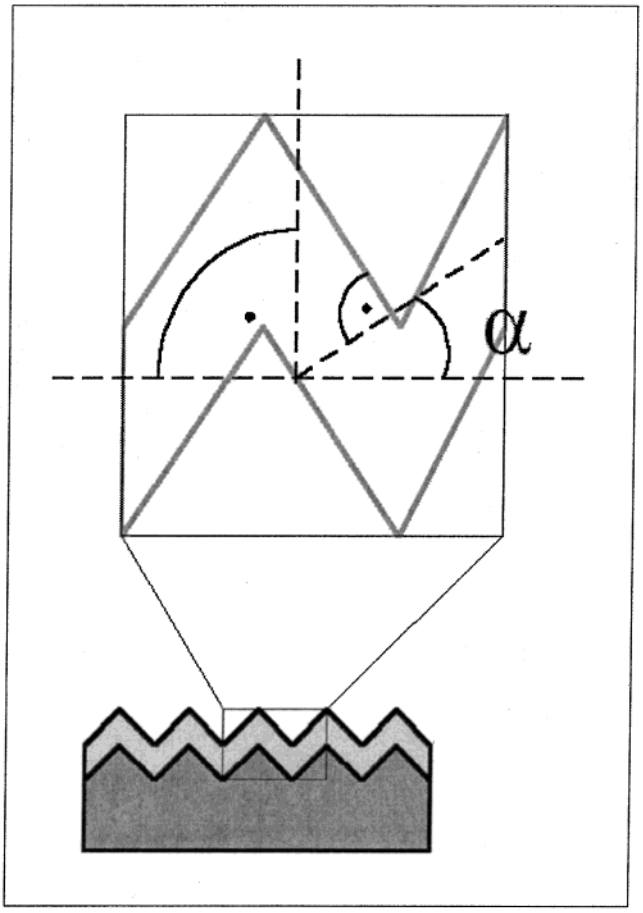


**Figure 13.** Idealized representation of the rough titanium (SLA) surface with a uniform local slope (angle α) of the surface relative to the average surface plane.

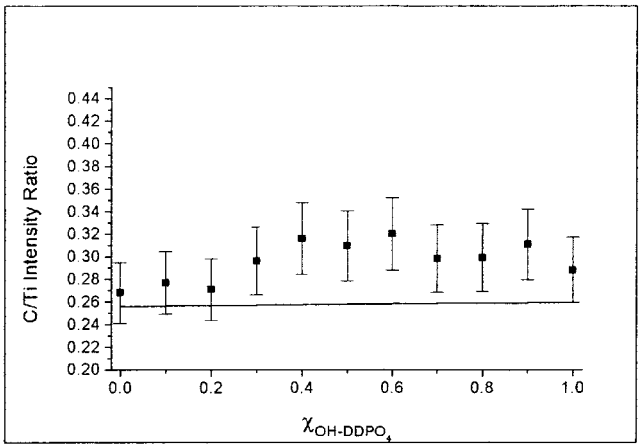


**Figure 14.** C(1s)/Ti(2p) XPS intensity ratios as function of the composition of the self-assembly solution, $\chi_{OH-DDPO_4}$ = [OH−$DDPO_4(NH_4)_2$]/{[OH−$DDPO_4(NH_4)_2$] + [$DDPO_4(NH_4)_2$]}, for the rough titanium metal (SLA) substrate. Experimental values are given as symbols together with the estimated error range. The line refers to calculated ratios assuming a density of 4.8 × $10^{14}$ molecules/$cm^2$ (effective surface) in the SAM layer (see text).

The advancing contact angles of 110−112° for the methyl-terminated self-assembled monolayer and of 55° for the hydroxy-terminated surfaces support the model of an organized layer with the −$CH_3$ and −OH end groups of the amphiphilic molecules being exposed to the ambient environment (vacuum, air, or water) and with the phosphate groups being oriented toward the substrate.

However, the experimentally observed advancing (but not the receding) contact angle of 50−55° for the hydroxy-terminated alkane phosphate SAM is significantly higher compared to that of a well-ordered hydroxyl-terminated alkanethiol film on gold or other hydrophilic surfaces, for which water contact angles below 20° have been reported.[5] Our hypothesis was that this observation is indicative of a comparably lower order for the hydroxy-terminated alkane phosphate SAM, thus partly exposing more hydrophobic $-CH_2-$ groups at the surface. In a companion paper,[22] the authors have determined order in the same type of SAMs using NEXAFS. Indeed, there is a clear trend to a continuously lower degree of molecular order in these SAMs (increased angle of orientation of the alkane chains relative to the surface normal) as the proportion of the hydroxy-terminated alkane phosphate in the mixed adlayer is increased.

The ToF-SIMS spectra show a clear difference between bare oxide and self-assembled substrates, and the observed secondary ion fragments of the SAM surfaces provide further evidence for this type of molecular organization at the titanium oxide surface. The XPS intensity-ratio calculations are in reasonably good agreement with the assumed model of the organophosphate molecules assembled in the form of a densely packed monolayer with an intermolecular distance of 0.49 nm and an average density of $4.8 \times 10^{14}$ molecules/cm$^2$ or 21 Å$^2$ per molecule, similar values having been reported for octadecyl phosphate monolayers on (amorphous) tantalum oxide surfaces[3,4] as well as for alkanethiols on gold (111).[1,5]

The water contact angles of the SAMs formed in the mixed OH−$DDPO_4$/$DDPO_4$ solutions provide evidence that there is a gradual change in the composition of the adlayer as the ratio of concentration in solution is changed. The quantification of the terminal −C−O−H functional group (XPS) and of the (M − H) (M = $DDPO_4$) mass fragment at the surface (ToF-SIMS), however, points to an adlayer composition that is richer in OH−$DDPO_4$ than would be expected from the solution composition (Figures 8 and 12).

The evolution of the advancing contact angles of SAMs deposited from mixed solutions may be compared with predictions from model equations describing micro- to macroscopically heterogeneous, two-component surface systems. Cassie has proposed the following equation for such systems:[27]

$$\cos\theta_{\text{Mixed-SAM}} = f_{\text{DDPO}_4}\cos\theta_{\text{DDPO}_4} + f_{\text{OH-DDPO}_4}\cos\theta_{\text{OH-DDPO}_4} \quad (15)$$

where $f_{\text{DDPO}_4}$ and $f_{\text{OH-DDPO}_4}$ denote the relative surface coverage due to $DDPO_4$ and OH−$DDPO_4$, respectively ($f_{\text{DDPO}_4} + f_{\text{OH-DDPO}_4} = 1$).

Israelachvili and Gee[28] have proposed a modified equation that accounts for surfaces that exhibit heterogeneities on a scale close to molecular dimensions. This is likely the case for the SAMs under investigation:

$$(1+\cos\theta_{\text{Mixed-SAM}})^2 = f_{\text{DDPO}_4}(1+\cos\theta_{\text{DDPO}_4})^2 + f_{\text{OH-DDPO}_4}(1+\cos\theta_{\text{OH-DDPO}_4})^2 \quad (16)$$

Both theoretical equations have been used to estimate the deviations of the surface composition from that of the solution, by plotting the mole fraction $f_{\text{OH-DDPO}_4}$ at the surface, as calculated by the Cassie and Israelachvili & Gee equations, against the solution mole fraction $\chi_{\text{OH-DDPO}_4}$. This is shown in Figure 15, together with the corresponding values based on the experimentally measured surface concentration of the −C−O−H terminal groups (Figure 12) and of the normalized peak signal of (M − H) (Figure 8). The different approaches all point to a preferential adsorption and assembly of the OH−$DDPO_4$ molecules.

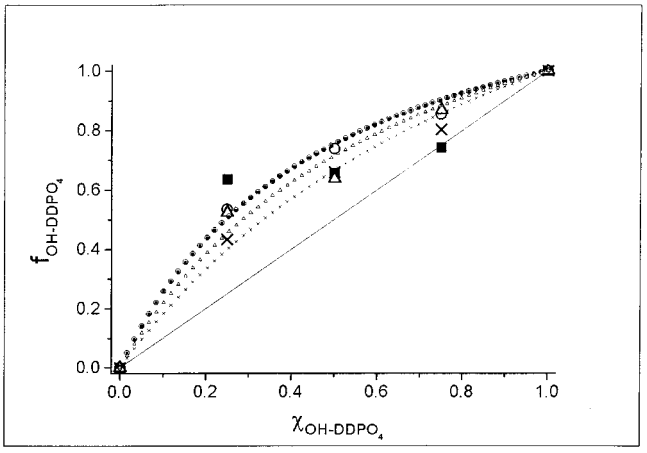


**Figure 15.** Plot of the molar fraction of OH−$DDPO_4$ in the SAM, $f_{\text{OH-DDPO}_4}$, against that of the self-assembly solution, $\chi_{\text{OH-DDPO}_4}$, using four different approaches: (a) Cassie equation for the contact angles of heterogeneous, patchy surfaces (○), (b) Israelachvili & Gee equation for the contact angle of heterogeneous systems at the molecular scale (×), (c) surface composition estimated via the concentration of the −C−O−H terminal groups at the surface (XPS, oxygen type 4) (■), and (d) surface composition estimated via the number of $DDPO_4$ molecules (ToF-SIMS, counts of (M − H) (M = $DDPO_4$)) (△). The straight line assumes a linear dependency between surface, $f_{\text{OH-DDPO4}}$, and solution, $\chi_{\text{OH-DDPO}_4}$, concentrations. Large markers are used for experimental data; small markers are calculated using eq 19 as a basis for the fitting function (see text). Surface: smooth titanium oxide coated Si wafer.

The data can be related to a SAM-formation model using the simplest approach, that is, a "Langmuir type" model where there is no interaction between the molecules, independent adsorption, and first-order kinetics. The kinetics of adsorption for $DDPO_4$ and OH−$DDPO_4$ can then be expressed as in eqs 17 and 18:

$$\frac{\mathrm{d}f_{\text{DDPO}_4}(t)}{\mathrm{d}t} = k_{\text{DDPO}_4} C^{\text{Solution}}_{\text{DDPO}_4}(1 - f_{\text{DDPO}_4}(t) - f_{\text{OH-DDPO}_4}(t)) \quad (17)$$

$$\frac{\mathrm{d}f_{\text{OH-DDPO}_4}(t)}{\mathrm{d}t} = k_{\text{OH-DDPO}_4} C^{\text{Solution}}_{\text{OHDDPO}_4}(1 - f_{\text{DDPO}_4}(t) - f_{\text{OH-DDPO}_4}(t)) \quad (18)$$

where $C^{\text{Solution}}_{\text{Molecule}}$ is the concentration of the molecule in the solution and $f_{\text{molecule}}$ is the partial coverage of the surface by the corresponding amphiphile. Since all of the solutions have a phosphate concentration of 0.5 mM, it is possible to substitute the concentration $C^{\text{Solution}}_{\text{Molecule}}$ by the corresponding mole fraction $\chi_{\text{OH-DDPO}_4}$. Solving the set of two differential equations and calculating the ratio $f_{\text{DDPO}_4}/f_{\text{OH-DDPO}_4}$, we obtain eq 19 for $t \rightarrow \infty$:

$$\frac{1 - f_{\text{OH-DDPO}_4}}{f_{\text{OH-DDPO}_4}} = k\frac{1 - \chi_{\text{OH-DDPO}_4}}{\chi_{\text{OH-DDPO}_4}} \quad (19)$$

(27) Cassie, A. B. D. *Discuss. Faraday Soc.* **1952**, *4*, 5041.
(28) Israelachvili, J. N.; Gee, M. L. *Langmuir* **1989**, *5*, 288.

**Table 8. Ratio of the First-Order Adsorption Rate Constants $k = k_{DDPO_4}/k_{OH-DDPO_4}$ Estimated by Fitting the Kinetic Model Equation to XPS Measurements, Contact-Angle Data, and ToF-SIMS Data**

| experimental method | evaluation technique | $k$ |
|---|---|---|
| ToF-SIMS | signal peak of (M − H) (M = $DDPO_4$) | 0.40 |
| XPS | quantification of COH using O(1s) peak component | 0.33 |
| contact-angle | Israelachvili equation | 0.33 |
| contact-angle | Cassie equation | 0.50 |

With $k = k_{DDPO_4}/k_{OH-DDPO_4}$, eq 19 can be solved for $f_{OH-DDPO_4}$ and used as a physical model based relation to fit the $f_{surface} = f_{surface}(\chi_{solution})$ curves presented in Figure 15, thus providing values for the ratio $k$ of the first-order adsorption rate constants. The $k$ values for the three different procedures to estimate $f_{surface}(\chi_{solution})$ are presented in Table 8. The fact that the values differ is not surprising, in view of the quite different experimental and theoretical approaches taken. The $k$ value based on the Cassie equation may be expected to be less appropriate than that of Israelachvili and Gee since the mixed SAMs are likely not to show any substantial segregation and formation of extended patches with different surface chemistries. Preliminary AFM studies have indeed not yielded any evidence of segregation. We may therefore conclude that the formation of mixed SAMs on flat titanium oxide and titanium metal surfaces from aqueous solutions of the two amphiphiles can be described by a simple first-order adsorption model with the adsorption rate for $OH-DDPO_4$ being 2−3 times higher than that of $DDPO_4$.

**4.2. Formation and Properties of Organophosphate SAMs on Rough (SLA) Surfaces.** The estimation of surface coverage and properties on rough surfaces, in comparison to the ideal smooth-surface case, is complicated by the influence of surface roughness on both the quantitative XPS intensities and the contact angles.

In terms of the XPS investigation, the intensity ratio Ti(2p)(oxide)/Ti(2p)(metal) (a sensitive measure of oxide film thickness) and the ratio C(1s)/Ti(2p) (a sensitive function of the self-assembly coverage) depend on the distribution of local slopes of the surface relative to the mean (macroscopic) surface plane (Figure 13). The SLA surface topography profiles are too complex to be used directly within the XPS model. Therefore, the assumption was made that a mean slope may be a reasonable first approximation to be introduced as a parameter in both intensity ratios mentioned above.

Assuming that the natural oxide film thickness of a flat CP titanium metal surface and of the rough SLA surface is the same, an approximate (mean) slope of 51.9° was calculated using eq 14. This value was then applied in the calculation of the C(1s)/Ti(2p) intensity ratio assuming the same specific SAM coverage as for the flat case, that is, a close-packed arrangement of the organophosphate molecules along the corrugated surface (corresponding to a coverage per geometric (flat) unit area that is higher than that of the smooth surface by the effective surface area factor). The calculated intensity ratios are plotted in Figure 14. Despite the crudeness of the assumption, the consistency of the results is promising, providing good evidence that the assumed model of a close-packed assembly of alkane phosphate molecules is indeed reasonable for the corrugated SLA surface.

The water contact angle is shown in Figure 5 as a function of the molar ratio $\chi_{OH-DDPO_4}$ of the solution. In comparison to the smooth surfaces, the advancing contact angles are significantly higher, by roughly 40°, on the SLA surfaces. Roughness is well-known to influence static contact angles. The vectors describing the interfacial tension are locally changed in direction, and the magnitudes of the vectors composing the well-known Young equation are correspondingly modified. The Young equation, which strictly holds only for ideally homogeneous and smooth surfaces, is therefore no longer applicable. Wenzel has proposed the use of a modified equation that considers the effective surface area,[29] also called roughness factor, $r$, as an explicit parameter describing the real, rough surface:

$$r(\gamma_S - \gamma_{SL}) = \gamma_{LV} \cos \theta_W \qquad (19)$$

where $\theta_W$ is now called the Wenzel angle and $r$ = specific surface/geometric surface ≥ 1. $\gamma_S$ is defined as the surface energy of the solid, $\gamma_{SL}$ is defined as the surface energy at the interface between solid and liquid, and $\gamma_{LV}$ is defined as the surface energy at the interface between liquid and vapor. The relation to the Young angle $\theta_Y$ is

$$\cos \theta_W = r \cos \theta_Y \qquad (20)$$

This approach predicts that the Wenzel contact angle should increase with roughness for Young angles greater than 90° and decrease for angles lower than 90°. Since in our experiments all advancing angles are higher for the rough case, even when the Young angle (smooth surface value) is below 90°, this model does not explain the evolution of the contact angles with $\chi_{solution}$ in our case.

A very simple, purely geometric argument is that for a surface with a pronounced local inclination of the surface relative to the average surface plane, the advancing water drop would preferentially wet the local surface regions pointing away from the droplet center, microscopically jumping from slope to adjacent slope as a consequence. This would mean that the advancing contact angle would be larger by approximately the mean angle of inclination of the surface. The 40° difference observed in advancing contact angle between SLA and the smooth surface is actually close to the value determined by XPS intensity-ratio considerations (52°, see above). However, the difference between advancing and receding contact angle (hysteresis) cannot be explained by this oversimplified model. Hysteresis may provide very useful information about the surface chemistry and structure if it can be treated with a suitable model. It has been discussed in terms of surface heterogeneities (chemical and morphological) and the existence of many metastable energy minima in the free energy versus contact angle dependence.[30] In addition, hysteresis information may contain kinetic contributions if surface chemical changes occur during the course of the wettability studies.

The behavior of very rough, high-aspect-ratio surfaces (such as the SLA) is most likely governed by pronounced heterogeneities. In the $DDPO_4$-rich case in particular, this likely means that the fine structure of the surface is not completely wetted, water being prevented from penetrating into the topographical features of the surface. The Cassie and Baxter equation[31,32] may describe such surfaces:

(29) Wenzel, R. N. *Ind. Eng. Chem.* **1936**, *28*, 988.
(30) Garbassi, F.; Morra, M.; Occhiello, E. *Polymer Surfaces*; John Wiley & Sons: New York, 1994; Chapter 4.
(31) Cassie, A. B. D.; Baxter, S. *Trans. Faraday Soc.* **1944**, *40*, 549.
(32) Cassie, A. B. D.; Baxter, S. *J. Text. Inst.* **1945**, *36*, T67.

$$\cos \theta_{CB} = f_1 \cos \theta_1 - f_2 \quad (21)$$

where the heterogeneity is due to the local water−surface contact area $f_1$ (with contact angle $\theta_1$) and local water/air contact areas $f_2$ (with $\theta_2$ assumed to be 180°, $\cos \theta_2 = -1$). For a pure $DDPO_4$ SAM on Ti(SLA), the effective surface contact area may thus be only 20% of the total area. In the hydrophobic case, the general behavior of such hydrophobic and rough surfaces is characterized by extremely high (ca. 140−170°) contact angles and, if studied as a function of surface roughness, a sudden decrease of hysteresis above a critical roughness, due to a sudden decrease of the energy barrier between metastable states.[31,32,33] This is the situation for highly nonwettable surfaces, where the water droplet can actually move almost unhindered along the surface, a concept used by nature in leaves ("Lotus effect"), feathers, and so forth, to prevent wetting and to reduce the risk of adhesion of particles, bacteria, and fungi ("self-cleaning" properties).[26] The left-hand side of Figure 5 certainly corresponds to this case with a high advancing contact angle of ca. 140−150° and a relatively small hysteresis, similar to that observed in etched, microscopically rough poly(tetrafluoroethylene) surfaces.[33] On surfaces with Young contact angles below 90°, there is a rapid increase of hysteresis as roughness is increased up to the point where penetration of water into the microscopic surface texture ("wicking") occurs, at which point the advancing angle decreases again and the receding angle essentially goes to zero. The mixed SAMs on SLA do indeed show an extreme jump from low (about 5−10°) to very pronounced hysteresis (about 110°) as the molar fraction $\chi_{OH-DDPO_4}$ reaches 0.2−0.25. In that sense, the observation of much higher hysteresis as the adlayer becomes more hydrophilic is in agreement with the general observations reported in the literature.[29] However, the reason for the sharp discontinuity is not known to us. It is rather unlikely that this discontinuity reflects the onset of wetting of the surface structures (at least not of the fine etch structure of pits with diameters in the range 0.5−2 $\mu$m). First, this would also have to result in abrupt changes of the advancing contact angle, and second, it is known that even quite low Young contact angles (i.e., moderately hydrophilic surfaces) are still effective in preventing wicking.

More work, including surface-tension measurements (e.g., via Wilhelmy balance investigations), will be needed to better explain the details of the behavior of mixed organophosphate SAMs on rough (e.g., SLA type) titanium (oxide) surfaces. The motivation for further investigation is twofold: we believe that the interfacial energetics is important in the context of protein adsorption and conformational effects and therefore highly relevant to the biomaterials area; second, the mixed $DDPO_4$/OH−$DDPO_4$ system, together with well-defined surface structures, is expected to be a useful model system for investigating surface/interface energetics with truly independent control of surface chemistry and topography.

(33) Lupis, H. C. O. *Chemical Thermodynamics of Materials*; North-Holland: New York, 1983; Chapter 23.

## 5. Conclusion

The technique of spontaneous organization of organophosphate molecules on titanium (oxide) surfaces is believed to have potential for the modification of titanium-based medical implants and devices with the aim of tailoring the surface chemistry (chemical or biological functionalities) to the particular needs of the application. It is a cost-effective technique (simple dipping process) but needs careful control of all relevant parameters, in particular in terms of cleanliness or purity of surfaces and materials used. Methyl- and hydroxy-terminated dodecyl phosphate were used as model systems to investigate self-assembly processes from aqueous solution onto titanium (oxide) surfaces. By using the technique of coadsorbed self-assembled monolayers, it was demonstrated that the technique allows the wettability of the surface to be tailored, not only in the case of smooth surfaces but also for high-surface-area materials, such as the SLA dental implant surface.

The technique also has applicability for basic studies. Wettability phenomena on surfaces of defined topography or roughness (including the observation of contamination-resistant, self-cleaning natural surfaces (Lotus effect)) could be studied much more systematically by having truly independent control over surface chemistry and topography.

In addition to tailoring wettability with alkyl phosphates, one could also impart further properties of interest in the fields of biomaterials and cell−surface interactions, including electric charges (e.g., by means of terminal amine, carboxylate, or phosphate functionalities) and biologically active groups such as poly(ethylene glycol), cell-adhesive peptides, or growth factors.

Further investigation should lead to a better understanding of the influence that minor changes in surface order have on adlayer properties such as resistance to recontamination or stability on contact with solutions of different compositions (water, buffer, etc.).

**Acknowledgment.** We acknowledge financial support by the International Team of Oral Implantology, ITI Foundation Research Committee, Waldenburg, Switzerland, N.P. Huang for her careful AFM measurements on the cleaned samples, and R. Hofer and S. DePaul for the scientific support.

LA011459P